

A Mathematical Framework Towards a Unified Set of Discontinuous State-Phase Hierarchical Time Operators for Computational Dynamics

R.Kanapady¹ and K.K.Tamma²

Abstract: Of general interest here is the time dimension aspect wherein discretized operators in time may be continuous or discontinuous; and of particular interest and focus here is the design of time discretized operators in the context of discontinuous state-phase for computational dynamics applications. Based on a generalized bi-discontinuous time weighted residual formulation, the design leading to a new unified set of hierarchical energy conserving and energy dissipating time discretized operators are developed for the first time that are fundamentally useful for time adaptive computations for dynamic problems. Unlike time discontinuous Galerkin approaches, the design is based upon a time discontinuous Petrov-Galerkin-like approach employing an asymptotic series type approximations for the state variables involving derivatives at the beginning of the time step. As a consequence, this enables to design methods that have spectral properties corresponding to the diagonal, first sub-diagonal and second sub-diagonal Padé entries. Thus, A -stable schemes of order $2q$, L -stable schemes of order $2q - 1$ and $2q - 2$ are obtained. The spectral equivalent algorithms to the diagonal Padé entry are energy conserving algorithms. The spectral equivalent algorithms to the first and second sub-diagonal Padé entries are energy dissipating algorithms with the property of asymptotic annihilation of the high frequency response. Additionally, these time operators naturally inherit a hierarchical structure that are extremely useful for time adaptive computations. Moreover, since Padé entries have the lowest relative error the developed schemes are optimal in terms of order of accuracy in time, dissipation, dispersion and zero-order displacement and velocity overshoot charac-

teristics.

keyword: Time discretized discontinuous operators; Generalized weighted residual approach; Hierarchical Time Formulations; Computational Dynamics

1 Introduction

For computational dynamics applications, the commonly employed time integration operators, when applied to the equations of motion in state space representation (two-field form or mixed or hybrid formulations) lead to the following amplifications of the errors as $d_{n+1} = R(z)d_n$ where $z = \lambda\Delta t$ and $R(z)$ is the so-called “stability function”. In the context of time continuous operators, for the explicit Euler method, trapezoidal and implicit midpoint rule, and the implicit Euler method, respectively, the stability functions are $R(z) = 1 + z$; $R(z) = (1 + z)/(1 - z)$ and $R(z) = 1/(1 - z)$. These are simply particular entries of the Padé table of the exponential map in which the numerator P and the denominator Q may be expressed in rational form as [Ehle (1969)]

$$R_{i,j}(z) = \frac{P_i(z)}{Q_j(z)} = \frac{\sum_{l=0}^j \frac{j!}{(j-l)!} \frac{(i+j-l)!}{(i+j)!} \frac{z^l}{l!}}{\sum_{l=0}^i \frac{i!}{(i-l)!} \frac{(i+j-l)!}{(i+j)!} \frac{(-z)^l}{l!}} \quad (1)$$

where i and j are the degrees of the polynomials of the numerator and denominator, respectively. It is a well known fact that for a given degree of the numerator and denominator the resulting approximation has the highest order of accuracy [Gragg (1972)] where the order of accuracy is given by $i + j$. In addition, all entries (i, j) of the Padé table of the exponential map, with $i < j$ (entries below diagonal) possess the asymptotic annihilation property. Time operators that possess this property asymptotically annihilate the high-frequency response, i.e., the spurious oscillations in the high frequency regime are eliminated after one time step. However, the famous conjecture of Ehle ([Ehle (1969)], p.65) which was proved

¹ Ph. D., Research Associate, Department of Mechanical Engineering, 111 Church Street S.E., University of Minnesota, MN, U.S.A., ramdev@me.umn.edu, Ph: 612-626-8101, Fax: 612-626-1596.

² Professor and Technical Director, Mechanical Engineering Department/Army High Performance Computing Research Center, 111 Church Street S.E., Technical Director, AHPCRC, University of Minnesota, MN, U.S.A. ktamma@tc.umn.edu, Ph: 612-626-8102, Fax: 612-626-1596.

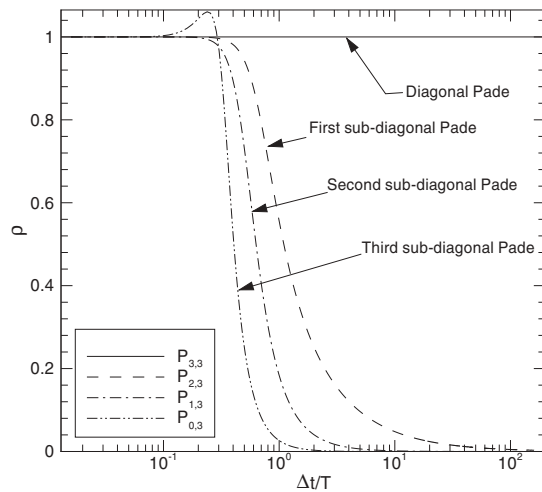


Figure 1 : Typical spectral curves for the diagonal, first sub-diagonal, second sub-diagonal and third sub-diagonal Padé exponential map substantiates that with the exception of the diagonal and the first and second lower sub-diagonals, no entry of the Padé table is A -stable for structural dynamics.

by Hairer and Warner [Hairer and Wanner (2000)] states that *with the exception of the diagonal and the first and second lower sub-diagonals, i.e., of $j - 2 \leq i \leq j$, no entry of the Padé table is A -stable* where A -stability is defined as $|R(z)| \leq 1$. This is also illustrated in the Fig. 1 where the spectral radius curve is plotted for a typical row of entries of the Padé table for structural dynamics. Figure 1 clearly indicates that only the diagonal and the first and second sub-diagonal entries of the Padé table are A -stable as illustrated by $\rho \leq 1$.

Thus, the above discussion clearly provides a motivation for the need to design time operators with properties equivalent to diagonal, the first lower sub-diagonal and the second lower sub-diagonal entries of the Padé table in a unified framework. Such algorithmic attributes are important for computational dynamics. Previous efforts [Hulbert (1992); Borri and Bottasso (1993); Li and Wiberg (1996); Wiberg and Li (1996); Chien and Wu (2001)] fail to provide a unified framework to simultaneously yield a unified set of computational algorithms that are spectrally equivalent to the diagonal, the first sub-diagonal, and the second sub-diagonal Padé approximations from time discontinuous formulations. Finally,

no framework exists to-date that simultaneously yields a hierarchical unified set of the same for time dependent adaptive computations.

Emanating from a generalized bi-discontinuous time weighted residual formulation, a new unified set of energy conserving and energy dissipating time discretized operators for the two-field form are presented here that are fundamentally useful for structural dynamic computations. Unlike the time discontinuous Galerkin approach [Hulbert (1992)], the design of the algorithms are based upon a time discontinuous Petrov-Galerkin-like approach with the particular notion of independent approximations of the state variables. The state variables specifically employ an asymptotic series type approximation involving values of derivatives of state variable at the beginning of time step. These latter approaches now readily enable the design of time discretized operators that have spectral properties corresponding to the diagonal, the first and second lower sub-diagonals of the Padé table entries. Thus, A -stable schemes of order $2q$, L -stable schemes of order $2q - 1$ and $2q - 2$ can be readily designed where q is the number of system solves. The time integration operators that are spectrally equivalent to the diagonal Padé table entries are termed energy conserving algorithms. The time integration operators that are spectrally equivalent to first and second sub-diagonal Padé table entries are energy dissipating algorithms with the property of asymptotic annihilation of the high-frequency response. Since Padé approximations have the lowest relative error, the present design of the time operators is optimal in terms of the order of accuracy in time, and numerical dissipation and dispersion with zero-order displacement and velocity overshoot characteristics. It is also noteworthy to point out that additionally, the integration operators that are spectrally equivalent to the diagonal, first sub-diagonal, and also the second sub-diagonal Padé exponential maps naturally inherit a hierarchical structure that is useful for enabling adaptive computations. The theoretical developments and stability, and convergence are also described for the various designs of time operators for computational dynamics.

The present exposition is organized as follows. Following the aforementioned brief introduction and motivation in Section 1, a description of the equations of motion and the weakforms considered is described in Section 2. In Section 3, the approximations of the weighted time fields

and state variables are described followed by the design of the time discontinuous operators in Section 4. In Section 5, the spectral analyses as related to the stability, consistency, numerical dissipation, numerical dispersion and overshoot behavior are presented for the developed time integrators followed by conclusions in Section 6.

2 Equations of Motion

The dynamic problems can be represented in configuration space representation (single-field or irreducible form), second-order ordinary differential equation system after the finite element discretization in space. These can be described in matrix form (strong form) as:

$$L(\mathbf{u}) - \mathbf{f} = 0; \quad \mathbf{u}(t_n) = \mathbf{u}_0; \quad \dot{\mathbf{u}}(t_n) = \dot{\mathbf{u}}_0 \quad (2)$$

where the operator $L(\mathbf{u})$ is given by $L(\mathbf{u}) \equiv \mathbf{M} \ddot{\mathbf{u}} + \mathbf{C} \dot{\mathbf{u}} + \mathbf{K} \mathbf{u} = \mathbf{f}$. \mathbf{M} , \mathbf{C} and \mathbf{K} are the respective mass, damping, and stiffness matrices, \mathbf{f} is the vector of externally applied forces, \mathbf{u} is the displacement vector, and $(\dot{\cdot})$ and $(\ddot{\cdot})$ denotes a single and double derivative with respect to time. The matrix \mathbf{M} is assumed to be symmetric positive-definite and matrices \mathbf{C} and \mathbf{K} are assumed to be symmetric semi-definite. For convenience in the theoretical design, we focus on an equivalent first-order system for structural dynamics where the second-order differential Eq. 2 is transformed into two first-order differential equations. Letting $\dot{\mathbf{u}} = \mathbf{v}$ and $\ddot{\mathbf{u}} = \dot{\mathbf{v}}$ in Eq. 2, the equivalent state-phase (two-field, first-order, reducible or mixed formulations) representation is given as

$$L(\mathbf{d}) - \mathbf{F} = 0; \quad \mathbf{d}(t_n) = \mathbf{d}_0 \quad (3)$$

where the operator $L(\mathbf{d})$ is given by

$$L(\mathbf{d}) \equiv \dot{\mathbf{d}} + \mathbf{A} \mathbf{d} = \mathbf{F} \quad (4)$$

and

$$\mathbf{d} = \begin{pmatrix} \mathbf{u} \\ \mathbf{v} \end{pmatrix}; \quad \mathbf{A} = \begin{bmatrix} \mathbf{0} & -\mathbf{I} \\ \mathbf{M}^{-1} \mathbf{K} & \mathbf{M}^{-1} \mathbf{C} \end{bmatrix}; \quad \mathbf{F} = \begin{pmatrix} \mathbf{0} \\ \mathbf{M}^{-1} \mathbf{f} \end{pmatrix} \quad (5)$$

Assuming an arbitrary virtual field or weighted time field, $\mathbf{w}(t)$, for enacting the time discretization process, the above semi-discretized system can be cast into the form:

$$(L(\mathbf{d}) - \mathbf{F}, \mathbf{w}) = 0; \quad \mathbf{d}(t_n) = \mathbf{d}_0 \quad \forall \mathbf{w} \in [t_n, t_{n+1}] \quad (6)$$

After integrating by parts, we have

$$(M(\mathbf{w}), \mathbf{d}) + \mathbf{w} \cdot \mathbf{d} \Big|_{t_n}^{t_{n+1}} - (\mathbf{F}, \mathbf{w}) = 0 \quad (7)$$

The solution of the adjoint equation $M(\mathbf{w}) \equiv \mathbf{w} \cdot \mathbf{A} - \dot{\mathbf{w}} = 0$ yields $\mathbf{w}(t) = \mathbf{w}_{exact}$ which when employed in Eq. 7 leads to the exact theoretical solution which is an exponential matrix representation. It is also evident from Eq. 7 that such a selection, does not necessitate the need to approximate the state variables as it is irrelevant [Tamma, Zhou, and Sha (2000)].

3 Approximation of Weighted Time Fields and State Variables

In this section, emanating from the exact weighted time fields, the degeneration process and the resulting consequence leading to and explaining the design of the so-called time integration operators involving a multiple system and a single solution step are described. The objectives and focus here is to first describe the underlying basis that can explain how to obtain the resulting approximations of the weighted time fields emanating from the exact weighted time fields, and also the imposed conditions for approximating the state variables and leading to the general design and framework of computational algorithms encompassing state-phase time discretized operators.

Consider the following transformation permitting the degeneration of the exact weighted time fields from the second-order tensor (matrix) representation to a first-order tensor (vector) as

$$\mathbf{w}_{exact} \rightarrow \mathbf{w}(\bar{\tau}) = \mathbf{w} \mathbf{t}(\bar{\tau})^T = \begin{bmatrix} w_{10} & \dots & w_{1p} \\ \vdots & \ddots & \vdots \\ w_{q0} & \dots & w_{qp} \end{bmatrix} \begin{pmatrix} \bar{\tau}^0 \\ \vdots \\ \bar{\tau}^p \end{pmatrix} \quad (8)$$

where $p \leq n$ and $p \geq q$. This can be written in an asymptotic series type expansion as

$$\mathbf{w}_{Asymp}(\bar{\tau}) = \mathbf{w}_n^+ + \dot{\mathbf{w}}_n^+ \bar{\tau} + \ddot{\mathbf{w}}_n^+ \bar{\tau}^2 + \dots + \mathbf{w}_n^{(p)+} \bar{\tau}^p \quad (9)$$

$$= \left[\mathbf{w}_n^+, \dot{\mathbf{w}}_n^+, \dots, \mathbf{w}_n^{(p)+} \right] \mathbf{t}(\bar{\tau})^T \quad (10)$$

$$= \mathbf{w} \mathbf{t}(\bar{\tau})^T \quad (11)$$

where $\mathbf{w}_n^+, \dot{\mathbf{w}}_n^+, \dots, \mathbf{w}_n^{(p)+}$ are vectors of $\text{span}\{\mathbf{w}\}$ which admits the set of all linear combination of $\bar{\tau}$ vectors

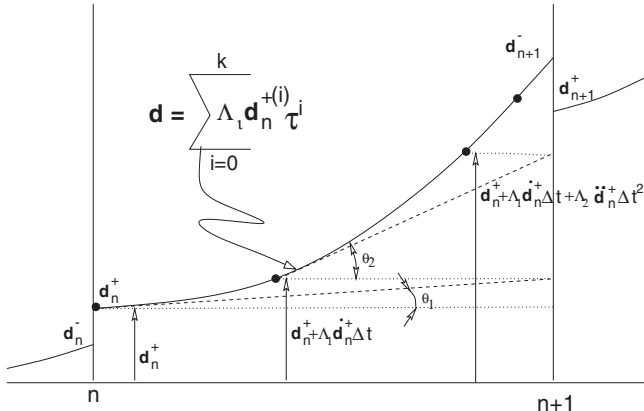


Figure 2 : Illustration of local approximation functions via the proposed asymptotic series.

$\mathbf{w}_n^{(j)+}$, $j = 0, 1, \dots, p$. $\mathbf{t}(\bar{\tau})^T$ is a vector of monomials $\bar{\tau}$. The size of these vectors is of order q and dictates the number of unknowns in the weakform. The dimension p dictates the other features of the time integration operators. The $(\cdot)_n^+$ representation for the vectors of $\text{span}(\mathbf{w})$ is employed here merely to be consistent with the representations of the time discontinuous formulations. If the vectors $\mathbf{w}_n^{(j)+}$, $j = 0, 1, \dots, p$ are linearly independent, then each vector of $\text{span}\{\mathbf{w}\}$ admits a unique expression as a linear combination of the $\mathbf{w}_n^{(j)+}$, $j = 0, 1, \dots, p$. Thus the set \mathbf{w} is then called a *basis* of the subspace $\text{span}\{\mathbf{w}\}$. This selection of \mathbf{w} now dictates the corresponding approximation for the state variables unlike employing \mathbf{w}_{exact} as evident from Eq. 7 (see also [Tamma, Zhou, and Sha (2000)]).

As a consequence, the corresponding local independent approximations to the state variables follows. Consider the following notion of a local asymptotic series type expansion for the approximation for $\bar{\mathbf{d}}$ as

$$\mathbf{d} \approx \bar{\mathbf{d}} = \mathbf{d}_{Asymp}(\bar{\tau}) = \sum_{i=0}^k \Lambda_i \mathbf{d}_n^{(i)+} \Delta t^i \bar{\tau}^i \quad (12)$$

where $\bar{\tau} \in (0, 1)$. Next, consider the following independent local approximation for $\dot{\bar{\mathbf{d}}}$ as

$$\dot{\mathbf{d}} \approx \dot{\bar{\mathbf{d}}} = \dot{\mathbf{d}}_{Asymp}(\bar{\tau}) = \sum_{i=1}^k \Lambda_{k+i} \mathbf{d}_n^{(i)+} \Delta t^{i-1} \bar{\tau}^{i-1} \quad (13)$$

where Λ_i , $i = 0, \dots, 2k$ are free parameters. Alternatively, one may consider the equations of motion given

by $\dot{\mathbf{d}} + \mathbf{A}\mathbf{d} - \mathbf{F} = 0$ for the approximation of the state variables. This implies that the state variable \mathbf{d} can also be independently approximated as $\dot{\mathbf{d}} = -\mathbf{A}\mathbf{d} + \mathbf{F}$, and results in

$$\dot{\bar{\mathbf{d}}} \approx \dot{\bar{\mathbf{d}}} = -\mathbf{A}\bar{\mathbf{d}} + \mathbf{F} = -\mathbf{A} \sum_{i=0}^k \Lambda_i \mathbf{d}_n^{(i)+} \Delta t^i \bar{\tau}^i + \mathbf{F} \quad (14)$$

Based on Eq. 12, for illustration, the relevant approximations of linear and quadratic forms are given by

$$\bar{\mathbf{d}}(\bar{\tau}) = \Lambda_0 \mathbf{d}_n^+ + \Lambda_1 \dot{\mathbf{d}}_n^+ \Delta t \bar{\tau}; \quad k = 1 \quad (15)$$

$$\bar{\mathbf{d}}(\bar{\tau}) = \Lambda_0 \mathbf{d}_n^+ + \Lambda_1 \dot{\mathbf{d}}_n^+ \Delta t \bar{\tau} + \Lambda_2 \ddot{\mathbf{d}}_n^+ \Delta t^2 \bar{\tau}^2; \quad k = 2 \quad (16)$$

Based on Eq. 13, the corresponding independent local approximations for $\dot{\bar{\mathbf{d}}}$, respectively yield

$$\dot{\bar{\mathbf{d}}}(\bar{\tau}) = \Lambda_2 \dot{\mathbf{d}}_n^+; \quad k = 1 \quad (17)$$

$$\dot{\bar{\mathbf{d}}}(\bar{\tau}) = \Lambda_3 \dot{\mathbf{d}}_n^+ + \Lambda_4 \ddot{\mathbf{d}}_n^+ \Delta t \bar{\tau}; \quad k = 2 \quad (18)$$

Alternatively, following Eq. 14, we can also have the independent local approximations for $\dot{\bar{\mathbf{d}}}$ as

$$\begin{aligned} \dot{\bar{\mathbf{d}}}(\bar{\tau}) &= -\mathbf{A}\bar{\mathbf{d}} + \mathbf{F} \\ &= -\mathbf{A}(\Lambda_0 \mathbf{d}_n^+ + \Lambda_1 \dot{\mathbf{d}}_n^+ \Delta t \bar{\tau}) + \mathbf{F}; \quad k = 1 \\ \dot{\bar{\mathbf{d}}}(\bar{\tau}) &= -\mathbf{A}\bar{\mathbf{d}} + \mathbf{F} \\ &= -\mathbf{A}(\Lambda_0 \mathbf{d}_n^+ + \Lambda_1 \dot{\mathbf{d}}_n^+ \Delta t \bar{\tau} + \Lambda_2 \ddot{\mathbf{d}}_n^+ \Delta t^2 \bar{\tau}^2) + \mathbf{F}; \quad k = 2 \end{aligned} \quad (19)$$

The load is approximated consistently upto l terms as

$$\mathbf{F} \approx \mathbf{F}_{Asymp}(\bar{\tau}) = \sum_{i=0}^l \theta_i \mathbf{F}_n^{(i)+} \Delta t^i \bar{\tau}^i; \quad (20)$$

where θ_i , $i = 1, \dots, l$ are free parameters. The order of approximation l for the load \mathbf{F} is taken to be one less than the order of accuracy of the time integration operator. That is, if $2k+2$, $2k+1$ and $2k$ are the order of accuracy of the time integration operator, then $l = 2k+1$, $2k$, and $2k-1$ respectively. Note that the size of the degenerated weighted time vector field, $\mathbf{w}(\bar{\tau})$, is the number of unknowns in the weakform. In designing time operators, there exists two fundamental aspects: (i) the aspect involving the “integrator” (which is associated with the semi-discretized equation system and the solution of

the corresponding equation system), and (ii) the aspect involving the design of “updates” (which are associated with computing or updating the primary state variables to advance to the end of the time step). In the text to follow, various bi-discontinuous (BD) integrators and the associated design updates with desired algorithmic attributes mimicking the diagonal, first and second sub-diagonal Padé entries are described.

4 Design of Time Integrator

The generalized bi-discontinuous weighted residual statement, with the limits of the integrals changed from (t_n, t_{n+1}) to $(0, 1)$ is described first.

If $L(\mathbf{d})$ is defined by Eq. 4, then the time weighted residual statement, Eq. 6, has the following two weighted residual statements as the equivalent time discontinuous weak form representations:

$$\begin{aligned} & (L(\bar{\mathbf{d}}) - \mathbf{F})\Delta t, \mathbf{w} \Big|_{I_+^-} \\ & + \mathbf{w}_{n+1} \cdot [\bar{\mathbf{d}}_{n+1}] + \mathbf{w}_n \cdot [\bar{\mathbf{d}}_n] = 0 \forall \mathbf{w} \in [0, 1] \end{aligned} \quad (21)$$

$$\begin{aligned} & (\bar{\mathbf{d}}' - \dot{\bar{\mathbf{d}}}, \hat{\mathbf{w}}) \Big|_{I_+^-} \\ & + \hat{\mathbf{w}}_{n+1} \cdot [\bar{\mathbf{d}}_{n+1}] + \hat{\mathbf{w}}_n \cdot [\bar{\mathbf{d}}_n] = 0 \forall \hat{\mathbf{w}} \in [0, 1] \end{aligned} \quad (22)$$

where $\bar{\mathbf{d}}$ and $\dot{\bar{\mathbf{d}}}$ are independent approximations to the solution \mathbf{d} and $\dot{\mathbf{d}}$ of $L(\mathbf{d}) - \mathbf{F} = 0$, $\bar{\mathbf{d}}'$ is the differentiation of $\bar{\mathbf{d}}$ with respect to t , and $[\cdot]$ is the temporal jump operator defined as $[\cdot] = (\cdot)^+ - (\cdot)^-$, $(\cdot)^\pm = (\cdot)(t_n^\pm) = \lim_{\varepsilon \rightarrow 0^\pm} (\cdot)(t_n + \varepsilon) \Rightarrow \mathbf{d}(t_n^-) = \mathbf{d}_0$, $(\cdot, \cdot)_{I_+^-}$ is the $L^2[t_n, t_{n+1}]$ inner product is defined by $(\mathbf{x}, \mathbf{y})_{I_+^-} = \int_{t_n^+}^{t_{n+1}^-} \mathbf{x}(t) \cdot \mathbf{y}(t) dt$, and $I_+^- \in (t_n^+, t_{n+1}^-)$.

4.1 Design of Integrator

Substituting the degenerated weighted time vector field, Eq. 8, and the approximations Eqs. 12 and 13 for $\bar{\mathbf{d}}$ and $\dot{\bar{\mathbf{d}}}$ respectively in the generalized bi-discontinuous weakform, Eq. 21, results in the following multiple system single solve ($q = k + 1$) representation of the time integration operator:

$$\bar{\mathbf{A}}\hat{\mathbf{d}} = \bar{\mathbf{F}} \quad (23)$$

where the integrator matrix $\bar{\mathbf{A}}$, the unknown vector $\hat{\mathbf{d}}$ and the effective load vector $\bar{\mathbf{F}}$ have the following representations:

$$\bar{\mathbf{A}} = \begin{bmatrix} r_{11}\mathbf{I} + s_{11}\mathbf{A}\Delta t & \dots & r_{1q}\mathbf{I} + s_{1q}\mathbf{A}\Delta t \\ \vdots & \ddots & \vdots \\ r_{q1}\mathbf{I} + s_{q1}\mathbf{A}\Delta t & \dots & r_{qq}\mathbf{I} + s_{qq}\mathbf{A}\Delta t \end{bmatrix} \quad (24)$$

$$\hat{\mathbf{d}} = \left(\mathbf{d}_n^+, \dot{\mathbf{d}}_n^+ \Delta t, \dots, \mathbf{d}_n^{(q)+} \Delta t^q \right)^\top \quad (25)$$

$$\bar{\mathbf{F}} = \mathbf{F}_\alpha + \mathbf{F}_\beta \quad (26)$$

$$\mathbf{F}_\alpha = (\alpha_1 \mathbf{d}_n^-, \dots, \alpha_q \mathbf{d}_n^-)^\top \quad (27)$$

$$\mathbf{F}_\beta = \Delta t \begin{pmatrix} \beta_{10}\mathbf{F}_n^+ + \beta_{11}\dot{\mathbf{F}}_n^+ + \dots + \beta_{1l}\mathbf{F}_n^{(l)+} \\ \vdots \\ \beta_{q0}\mathbf{F}_n^+ + \beta_{q1}\dot{\mathbf{F}}_n^+ + \dots + \beta_{ql}\mathbf{F}_n^{(l)+} \end{pmatrix} \quad (28)$$

$$\mathbf{F}_n^{(j)+} = \begin{pmatrix} 0 \\ \mathbf{M}^{-1}\mathbf{f}_n^{(j)+} \end{pmatrix} \quad j = 0, 1, \dots, l \quad (29)$$

with the coefficients in the above integrator given by

$$\mathbf{r} := [r_{ij}] = \begin{cases} w_{i0} & j = 1 \\ \Lambda_{k+j-1} \int_{0^+}^{1^-} w_i \bar{\tau}^{j-2} d\bar{\tau} & 2 \leq j \leq q = k+1 \end{cases} \quad (30)$$

$$\mathbf{s} := [s_{ij}] = \Lambda_{j-1} \int_{0^+}^{1^-} w_i \bar{\tau}^{j-1} d\bar{\tau} \quad 1 \leq j \leq q = k+1 \quad (31)$$

$$\boldsymbol{\alpha} := [\alpha_i] = w_{i0} \quad (32)$$

$$\boldsymbol{\beta} := [\beta_{ij}] = \theta_j \Delta t^j \int_{0^+}^{1^-} w_i \bar{\tau}^j \quad 0 \leq j \leq l; \quad (33)$$

$$\boldsymbol{\gamma} := [\gamma_{ij}] = \sum_{j=0}^p w_{ij} \quad (34)$$

Once the unknown quantities $(\mathbf{d}_n^+, \dot{\mathbf{d}}_n^+ \Delta t, \dots, \mathbf{d}_n^{(q)+} \Delta t^q)$ are found employing the integrator, Eq. 23, the end conditions, namely, \mathbf{d}_{n+1}^+ can be found employing the design updates as described next.

4.2 Design of Updates

To design the updates, consider the weakform in Eq. 22 of the proposed weighted residual statements relating to Eq. 6. Integrating by parts the term associated with $\bar{\mathbf{d}}'$ in Eq. 22, we have

$$\mathbf{d}_{n+1}^+ \cdot \hat{\mathbf{w}}_{n+1} = \mathbf{d}_n^- \cdot \hat{\mathbf{w}}_n + \left(\mathbf{d}, \hat{\mathbf{w}} \right)_{I_{0^+}^{1^-}} + \left(\dot{\mathbf{d}} \Delta t, \hat{\mathbf{w}} \right)_{I_{0^+}^{1^-}} \quad (35)$$

Consider the degenerated weighted time field for the updates, the span of which is given by

$$\text{span}\{\hat{\mathbf{w}}\} = [\hat{w}_0 \quad \dots \quad \hat{w}_{\hat{p}}] \quad (36)$$

At this point, consider the two alternatives in Eqs. 12, 13 for the approximation of $\bar{\mathbf{d}}$ in Eq. 35. First, Eq. 13 is considered and then Eq. 14 is considered. Substituting the weighted time fields, Eq. 36 and the local independent approximations, Eqs. 12 and 13 for $\bar{\mathbf{d}}$ and $\dot{\bar{\mathbf{d}}}$ respectively in Eq. 35, yields the following design for the updates:

$$\mathbf{d}_{n+1}^+ = \lambda_0 \mathbf{d}_n^- + \mathbf{I} \sum_{i=0}^k \lambda_{i+1} \mathbf{d}_n^{(i)+} \Delta t^i \quad (37)$$

Alternatively, substituting the weighted time fields Eq. 36 and the local independent approximations Eqs. 12 and 14 instead for $\bar{\mathbf{d}}$ and $\dot{\bar{\mathbf{d}}}$ respectively in Eq. 35, yields the following design for the updates:

$$\mathbf{d}_{n+1}^+ = \lambda_0 \mathbf{d}_n^- - \Delta t (\mathbf{A} \sum_{i=0}^k \lambda_{i+1} \mathbf{d}_n^{(i)+} \Delta t^i + \int_{0^+}^{1^-} \hat{\mathbf{w}} \mathbf{F} d\bar{\tau}) \quad (38)$$

The above two distinct designs for the updates, namely, Eqs. 37 and 38 can be combined with a generic matrix \mathbf{A}_1 instead \mathbf{I} and \mathbf{A} into one as

$$\mathbf{d}_{n+1}^+ = \lambda_0 \mathbf{d}_n^- + \mathbf{A}_1 \sum_{i=0}^k \lambda_{i+1} \mathbf{d}_n^{(i)+} \Delta t^i + \lambda_{k+2} (\Delta t \int_{0^+}^{1^-} \hat{\mathbf{w}} \mathbf{F} d\bar{\tau}) \quad (39)$$

where

$$\mathbf{A}_1 = \begin{cases} \mathbf{I} & \text{or} \\ -\mathbf{A} \Delta t & \end{cases} \quad (40)$$

$$\lambda_i = \begin{cases} \frac{w_0}{\sum_{j=0}^q \hat{w}_j} & i = 0 \\ \frac{\Lambda_1 \int_{0^+}^{1^-} \hat{w} d\bar{\tau}}{\sum_{j=0}^q \hat{w}_j} & i = 1 \\ \frac{\int_{0^+}^{1^-} (\Lambda_{i-1} \hat{w} \bar{\tau}^{i-1} + \Lambda_{k+i} \hat{w} \bar{\tau}^{i-2}) d\bar{\tau}}{\sum_{j=0}^q \hat{w}_j}; & 2 \leq i \leq k+1 \\ 0 & \text{or } 1 & i = k+2 \end{cases} \quad (41)$$

In the following text, the algorithmic discrete numerically assigned [DNA] markers, namely, the coefficients $(\mathbf{w}, \hat{\mathbf{w}}, \Lambda, \lambda)$, for the various time integration operators equivalent to the diagonal, the first sub-diagonal and the second sub-diagonal follow next, and involve relationships to $\mathbf{r}, \mathbf{s}, \boldsymbol{\alpha}, \boldsymbol{\beta}$ that are unique for a particular algorithm and serve as the algorithm's signature (i.e. the $\mathbf{w}, \hat{\mathbf{w}}, \Lambda$ and λ must satisfy the unique relations).

4.3 $\mathbf{BD}_{q,q}$ Algorithms: $q = k + 1, p = k + 1, \hat{p} = p$

BD_{2,2}: The selected algorithmic [DNA] markers in Eq. 23 are as follows ($k = 1$):

$$\begin{aligned} \text{span}\{\mathbf{w}\} &= \begin{bmatrix} w_{10} & w_{11} & w_{12} \\ w_{20} & w_{21} & w_{22} \end{bmatrix} \\ &= \begin{bmatrix} 1 & -1 & 0 \\ 1 & 0 & -1 \end{bmatrix} \end{aligned} \quad (42)$$

$$\begin{aligned} \boldsymbol{\Lambda} &= \{\Lambda_0, \Lambda_1, \Lambda_2\} \\ &= \{1, 1, 1\} \end{aligned} \quad (43)$$

$$\begin{aligned} \text{span}\{\hat{\mathbf{w}}\} &= [\hat{w}_{10} \quad \hat{w}_{11} \quad \hat{w}_{12}] \\ &= [1 \quad 0 \quad 0] \\ \rightarrow \boldsymbol{\lambda} &= \{\lambda_0, \lambda_1, \lambda_2\} \\ &= \{1, 1, \frac{1}{2}\} \end{aligned} \quad (44)$$

The resulting coefficients of the time integrator $\bar{\mathbf{A}}$ and $\bar{\mathbf{F}}$ are as follows:

$$\begin{aligned} \mathbf{r} &= \begin{bmatrix} 1 & \frac{1}{2} \\ 1 & \frac{2}{3} \end{bmatrix}; \quad \mathbf{s} = \begin{bmatrix} \frac{1}{2} & \frac{1}{6} \\ \frac{2}{3} & \frac{1}{4} \end{bmatrix} \\ \boldsymbol{\alpha} &= \begin{bmatrix} 1 \\ 1 \end{bmatrix}; \quad \boldsymbol{\beta} = \begin{bmatrix} \frac{1}{2} & \frac{1}{6} \\ \frac{2}{3} & \frac{1}{4} \end{bmatrix} \end{aligned} \quad (45)$$

BD_{3,3}: The selected algorithmic [DNA] markers are as follows ($k = 2$):

$$\begin{aligned} \text{span}\{\mathbf{w}\} &= \begin{bmatrix} w_{10} & w_{11} & w_{12} & w_{13} \\ w_{20} & w_{21} & w_{22} & w_{13} \\ w_{30} & w_{31} & w_{32} & w_{13} \end{bmatrix} \\ &= \begin{bmatrix} 1 & -1 & 0 & 0 \\ 1 & 0 & -1 & 0 \\ 1 & 0 & 0 & -1 \end{bmatrix} \end{aligned} \quad (46)$$

$$\begin{aligned} \boldsymbol{\Lambda} &= \{\Lambda_0, \Lambda_1, \Lambda_2, \Lambda_3, \Lambda_4\} \\ &= \{1, 1, \frac{1}{2}, 1, \frac{1}{2}\} \end{aligned} \quad (47)$$

$$\begin{aligned} \text{span}\{\hat{\mathbf{w}}\} &= [\hat{w}_{10} \quad \hat{w}_{11} \quad \hat{w}_{12} \quad \hat{w}_{13}] \\ &= [1 \quad 0 \quad 0 \quad 0] \\ \rightarrow \boldsymbol{\lambda} &= \{\lambda_0, \lambda_1, \lambda_2, \lambda_3\} \\ &= \{1, 1, \frac{1}{2}, \frac{1}{6}\} \end{aligned} \quad (48)$$

The resulting coefficients of the time integrator $\bar{\mathbf{A}}$ and $\bar{\mathbf{F}}$

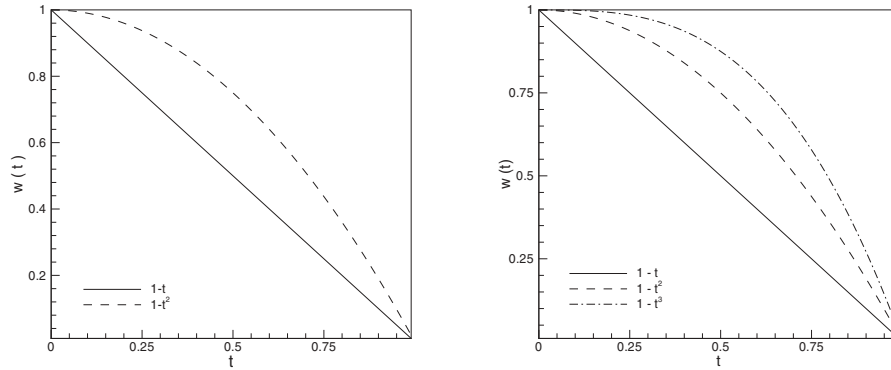


Figure 3 : Weighted time fields \mathbf{w} (test functions) for linear and quadratic trial functions for $BD_{q,q}$ time operators.

are as follows:

$$\mathbf{r} = \begin{bmatrix} 1 & \frac{1}{6} & \frac{1}{10} \\ 1 & \frac{1}{4} & \frac{3}{10} \\ 1 & \frac{1}{4} & \frac{3}{10} \end{bmatrix}; \quad \mathbf{s} = \begin{bmatrix} \frac{1}{6} & \frac{1}{4} & \frac{1}{24} \\ \frac{1}{4} & \frac{1}{4} & \frac{1}{15} \\ \frac{1}{4} & \frac{3}{10} & \frac{1}{12} \end{bmatrix} \quad (49)$$

$$\boldsymbol{\alpha} = \begin{bmatrix} 1 \\ 1 \\ 1 \end{bmatrix}; \quad \boldsymbol{\beta} = \begin{bmatrix} \frac{1}{2} & \frac{1}{6} & \frac{1}{24} \\ \frac{1}{3} & \frac{1}{4} & \frac{1}{15} \\ \frac{1}{4} & \frac{3}{10} & \frac{1}{12} \end{bmatrix}$$

The resulting coefficients of the time integrator $\bar{\mathbf{A}}$ and $\bar{\mathbf{F}}$ in Eq. 23 are as follows:

$$\mathbf{r} = \begin{bmatrix} 1 & \frac{1}{2} \\ 0 & \frac{1}{2} \end{bmatrix}; \quad \mathbf{s} = \begin{bmatrix} \frac{1}{2} & \frac{1}{3} \\ \frac{1}{2} & \frac{1}{3} \end{bmatrix} \quad (54)$$

$$\boldsymbol{\alpha} = \begin{bmatrix} 1 \\ 0 \end{bmatrix}; \quad \boldsymbol{\beta} = \begin{bmatrix} \frac{1}{2} & \frac{1}{3} \\ \frac{1}{2} & \frac{1}{3} \end{bmatrix}$$

The weighted time fields \mathbf{w} for the BD_{22} and BD_{33} time integration operators that are equivalent to the diagonal Padé table entries are depicted in Fig. 3a and 3b, respectively.

$BD_{2,3}$: The selected algorithmic [DNA] markers are as follows ($k = 2$):

4.4 $BD_{q-1,q}$ Algorithms: $q = k + 1, p = k + 2, \hat{p} = p$

$BD_{1,2}$: The selected algorithmic [DNA] markers are as follows ($k = 1$):

$$\text{span}\{\mathbf{w}\} = \begin{bmatrix} w_{10} & w_{11} & w_{12} & w_{13} \\ w_{20} & w_{21} & w_{22} & w_{13} \end{bmatrix}$$

$$= \begin{bmatrix} 1 & -3 & 12 & -10 \\ 0 & -2 & 12 & -10 \end{bmatrix}$$

$$\boldsymbol{\Lambda} = \{\Lambda_0, \Lambda_1, \Lambda_2\}$$

$$= \{1, 1, 1\}$$

$$\text{span}\{\hat{\mathbf{w}}\} = \begin{bmatrix} \hat{w}_{10} & \hat{w}_{11} & \hat{w}_{12} & \hat{w}_{13} \\ 0 & 1 & 0 & 0 \end{bmatrix}$$

$$\rightarrow \lambda = \{\lambda_0, \lambda_1, \lambda_2\}$$

$$= \{0, 1, 1\}$$

$$(50) \quad \text{span}\{\hat{\mathbf{w}}\} = \begin{bmatrix} \hat{w}_{10} & \hat{w}_{11} & \hat{w}_{12} & \hat{w}_{13} & \hat{w}_{14} \end{bmatrix}$$

$$= \begin{bmatrix} 0 & 0 & 1 & 0 & 0 \end{bmatrix} \quad (57)$$

$$\rightarrow \lambda = \{\lambda_0, \lambda_1, \lambda_2, \lambda_3\}$$

$$= \{0, 1, 1, \frac{1}{2}\} \quad (58)$$

(53) The resulting coefficients of the time integrator $\bar{\mathbf{A}}$ and $\bar{\mathbf{F}}$

$$\text{span}\{\mathbf{w}\} = \begin{bmatrix} w_{10} & w_{11} & w_{12} & w_{13} & w_{14} \\ w_{20} & w_{21} & w_{22} & w_{13} & w_{24} \\ w_{30} & w_{31} & w_{32} & w_{33} & w_{34} \end{bmatrix}$$

$$= \begin{bmatrix} 1 & 4 & -30 & 60 & -35 \\ 0 & 5 & -30 & 60 & -35 \\ 0 & 4 & -29 & 60 & -35 \end{bmatrix} \quad (55)$$

$$\boldsymbol{\Lambda} = \{\Lambda_0, \Lambda_1, \Lambda_2, \Lambda_3, \Lambda_4\}$$

$$= \{1, 1, \frac{1}{2}, 1, \frac{1}{2}\} \quad (56)$$

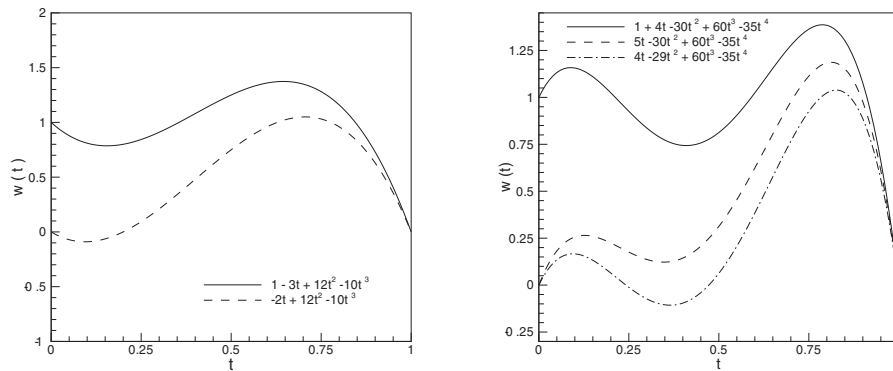


Figure 4 : Weighted time fields w (test functions) for linear and quadratic trial functions for $BD_{q-1,q}$ time operators.

in Eq. 23 are as follows:

$$\mathbf{r} = \begin{bmatrix} 1 & 1 & \frac{1}{2} \\ 0 & \frac{1}{2} & \frac{1}{3} \\ 0 & \frac{1}{3} & \frac{1}{4} \end{bmatrix}; \quad \mathbf{s} = \begin{bmatrix} 1 & \frac{1}{2} & \frac{1}{6} \\ \frac{1}{2} & \frac{1}{3} & \frac{1}{8} \\ \frac{1}{3} & \frac{1}{4} & \frac{1}{10} \end{bmatrix} \quad (59)$$

$$\boldsymbol{\alpha} = \begin{bmatrix} 1 \\ 0 \\ 0 \end{bmatrix}; \quad \boldsymbol{\beta} = \begin{bmatrix} 1 & \frac{1}{2} & \frac{1}{6} \\ \frac{1}{2} & \frac{1}{3} & \frac{1}{8} \\ \frac{1}{3} & \frac{1}{4} & \frac{1}{10} \end{bmatrix}$$

The resulting coefficients of the time integrator $\bar{\mathbf{A}}$ and $\bar{\mathbf{F}}$ in Eq. 23 are as follows:

$$\mathbf{r} = \begin{bmatrix} 1 & 1 \\ 0 & \frac{1}{2} \end{bmatrix}; \quad \mathbf{s} = \begin{bmatrix} 1 & \frac{1}{2} \\ \frac{1}{2} & \frac{1}{2} \end{bmatrix} \quad (64)$$

$$\boldsymbol{\alpha} = \begin{bmatrix} 1 \\ 0 \end{bmatrix}; \quad \boldsymbol{\beta} = \begin{bmatrix} 1 & \frac{1}{2} \\ \frac{1}{2} & \frac{1}{2} \end{bmatrix}$$

The weighted time fields w for the BD_{12} and BD_{23} time integration operators that are equivalent to the first lower sub-diagonal Padé table entries are depicted in Fig. 4a and 4b, respectively.

BD_{1,3}: The selected algorithmic [DNA] markers are as follows ($k = 2$):

4.5 $BD_{q-2,q}$ Algorithms: $q = k + 1, p = k + 2, \hat{p} = p$

BD_{0,2}: The selected algorithmic [DNA] markers are as follows ($k = 1$):

$$\text{span}\{\mathbf{w}\} = \begin{bmatrix} w_{10} & w_{11} & w_{12} & w_{13} \\ w_{20} & w_{21} & w_{22} & w_{23} \end{bmatrix} = \begin{bmatrix} 1 & -3 & 12 & -10 \\ 0 & -12 & 42 & -30 \end{bmatrix} \quad (60)$$

$$\Lambda = \{\Lambda_0, \Lambda_1, \Lambda_2\} = \{1, 1, 1\} \quad (61)$$

$$\text{span}\{\hat{\mathbf{w}}\} = \begin{bmatrix} \hat{w}_{10} & \hat{w}_{11} & \hat{w}_{12} & \hat{w}_{13} \\ 0 & 1 & 0 & 0 \end{bmatrix} \quad (62)$$

$$\rightarrow \lambda = \{\lambda_0, \lambda_1, \lambda_2\} = \{0, 1, 1\} \quad (63)$$

$$\text{span}\{\mathbf{w}\} = \begin{bmatrix} w_{10} & w_{11} & w_{12} & w_{13} & w_{14} \\ w_{20} & w_{21} & w_{22} & w_{23} & w_{24} \\ w_{30} & w_{31} & w_{32} & w_{33} & w_{34} \end{bmatrix} = \begin{bmatrix} 1 & 4 & -30 & 60 & -35 \\ 0 & 30 & -210 & 390 & -210 \\ 0 & 105 & -750 & 1380 & -735 \end{bmatrix} \quad (65)$$

$$\Lambda = \{\Lambda_0, \Lambda_1, \Lambda_2, \Lambda_3, \Lambda_4\} = \{1, 1, \frac{1}{2}, 1, \frac{1}{2}\} \quad (66)$$

$$\text{span}\{\hat{\mathbf{w}}\} = \begin{bmatrix} \hat{w}_{10} & \hat{w}_{11} & \hat{w}_{12} & \hat{w}_{13} & \hat{w}_{14} \\ 0 & 0 & 1 & 0 & 0 \end{bmatrix} \quad (67)$$

$$\rightarrow \lambda = \{\lambda_0, \lambda_1, \lambda_2, \lambda_3\} = \{0, 1, 1, \frac{1}{2}\} \quad (68)$$

(63) The resulting coefficients of the time integrators $\bar{\mathbf{A}}$ and $\bar{\mathbf{F}}$

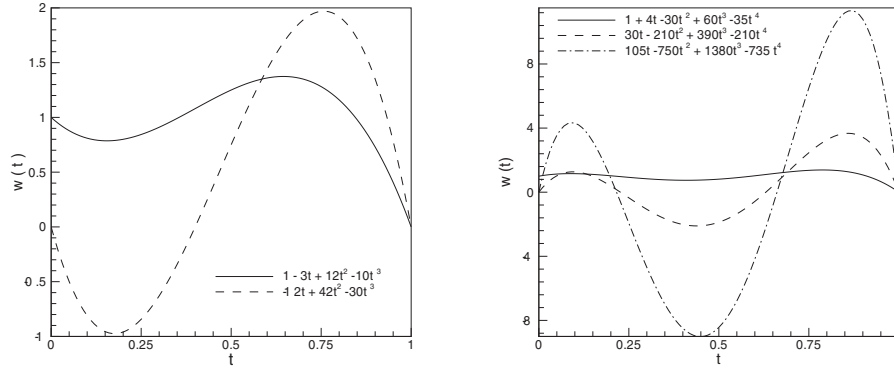


Figure 5 : Weighted time field \mathbf{w} (test functions) for linear and quadratic trial functions for $BD_{q-2,q}$ time operators.

in Eq. 23 are as follows:

$$\mathbf{r} = \begin{bmatrix} 1 & 1 & \frac{1}{2} \\ 0 & \frac{1}{2} & \frac{1}{2} \\ 0 & \frac{1}{2} & 1 \end{bmatrix}; \quad \mathbf{s} = \begin{bmatrix} 1 & \frac{1}{2} & \frac{1}{6} \\ \frac{1}{2} & \frac{1}{2} & \frac{1}{4} \\ \frac{1}{2} & 1 & \frac{5}{8} \end{bmatrix} \quad (69)$$

$$\boldsymbol{\alpha} = \begin{bmatrix} 1 \\ 0 \\ 0 \end{bmatrix}; \quad \boldsymbol{\beta} = \begin{bmatrix} 1 & \frac{1}{2} & \frac{1}{6} \\ \frac{1}{2} & \frac{1}{2} & \frac{1}{4} \\ \frac{1}{2} & 1 & \frac{5}{8} \end{bmatrix}$$

The weighted time fields \mathbf{w} for the BD_{02} and BD_{13} time operator that are equivalent to second lower sub-diagonal Padé table entries are depicted in Fig. 5a and 5b, respectively.

Particularly note that the time integration operator coefficients, namely $\mathbf{r}, \mathbf{s}, \boldsymbol{\alpha}$ and $\boldsymbol{\beta}$ for the $BD_{q,q}$, $BD_{q-1,q}$ and $BD_{q-2,q}$ have a hierarchical structure. That is, the time operator coefficients of the $BD_{2,2}$ operator is contained in the $BD_{3,3}$ operator, and likewise the $BD_{1,2}$ and $BD_{0,2}$ operators are contained in the $BD_{2,3}$ and $BD_{1,3}$ operators which implies that the lower order time integrators are contained in the high-order time integrators. The resulting design and such features provide a unified framework for a concise implementation and are useful in time adaptive computations to consistently increase the order of accuracy to arbitrary high-order as required by the problem at hand. Thus, in general, the design of the present bi-discontinuous time integration operators $BD_{i,j}, j = 2, 3; j-2 \leq i \leq j$ of arbitrary order that are equivalent to the Padé table entries $(i, j), j = 2, 3; j-2 \leq i \leq j$ can be summarized as follows.

Time integrator

Integrator:

$$\overline{\mathbf{A}} \hat{\mathbf{d}} = \overline{\mathbf{F}}$$

where

$$\hat{\mathbf{d}} = \begin{pmatrix} \mathbf{d}_n^+ \\ \vdots \\ \mathbf{d}_n^{(q)+} \Delta t^q \end{pmatrix}$$

$$\overline{\mathbf{A}} = \begin{bmatrix} r_{11}\mathbf{I} + s_{11}\mathbf{A}\Delta t & \dots & r_{1q}\mathbf{I} + s_{1q}\mathbf{A}\Delta t \\ \vdots & \ddots & \vdots \\ r_{11}\mathbf{I} + s_{11}\mathbf{A}\Delta t & \dots & r_{qq}\mathbf{I} + s_{qq}\mathbf{A}\Delta t \end{bmatrix};$$

$$\overline{\mathbf{F}} = \begin{pmatrix} \alpha_1 \mathbf{d}_n^- \\ \vdots \\ \alpha_q \mathbf{d}_n^- \end{pmatrix} + \Delta t \begin{pmatrix} \beta_{10}\mathbf{F}_n^+ + \dots + \beta_{1l}\mathbf{F}_n^{(l)+} \\ \vdots \\ \beta_{q0}\mathbf{F}_n^+ + \dots + \beta_{ql}\mathbf{F}_n^{(l)+} \end{pmatrix};$$

Design updates:

$$\mathbf{d}_{n+1}^+ = \lambda_0 \mathbf{d}_n^- + \mathbf{A}_1 \sum_{i=0}^k \lambda_{i+1} \mathbf{d}_n^{(i)+} \Delta t^i + \lambda_{k+2} \left(\int \hat{\mathbf{w}} \mathbf{F} d\bar{\tau} \right)$$

(69)

Note that the above time integration operator represents the integrators equivalent to all entries of the Padé table $(i, j), i \leq j$. Since $0 \leq i \leq j-2$ does not have an A -stable property, as pointed out earlier, the selection of the algorithmic [DNA] markers, namely, $(\mathbf{w}, \hat{\mathbf{w}}, \Lambda, \lambda)$ for these integrators is not derived here. Depending upon the representation selected for the matrix operator \mathbf{A} , the present design of BD time integration operators are applicable to

structural dynamics or Hamiltonian systems. In such situations, the primary state variable \mathbf{d} constitutes the displacement \mathbf{u} and velocity $\dot{\mathbf{u}}$ for structural dynamics, and displacement \mathbf{u} and momenta \mathbf{p} for the Hamiltonian system. It is also important to note here that the BD time integration operators are indeed applicable to the form of the semi-discrete first-order initial value problem having commonalities for applications in heat conduction and convection/diffusion type problems.

5 Spectral analysis

In this section, the spectral analyses as related to the stability, consistency, numerical dissipation, numerical dispersion and overshoot behavior are presented for the above developed integrators.

5.1 Stability

Here we derive the stability polynomial expression of the $BD_{i,j}$ integrators. For the system of first-order equations, the corresponding scalar equation after employing the eigenmodes to decouple the Eq. 3 (this also satisfies the Lax equivalence theorem) is given by

$$\dot{d} + \lambda d = 0; \quad d(0) = d_0 \quad (70)$$

where $\lambda = \pm i\omega$. For stability analysis, the end condition d_{n+1}^+ for the current time interval is expressed in terms of the end condition of the previous time interval d_n^- . This can be written in the form:

$$d_{n+1}^+ = A_{BD} d_n^- \quad (71)$$

where A_{BD} is the amplification factor for the bi-discontinuous time integrators. For all the $BD_{i,j}$ integrators described, the amplification factor can be derived as follows. Defining $\lambda\Delta t = z$, the unknowns within the time interval such as $d_n^+, d_n^-, \dots, d^{(q)+}$ are solved first employing the integrator $BD_{i,j}$ and then substituting these solved variables into the update equation to get the representation of the form Eq. 71. For the various integrators described earlier, the amplification factors can be respectively given as:

$$A_{BD_{2,2}} = \frac{1 - \frac{1}{2}z + \frac{1}{12}z^2}{1 + \frac{1}{2}z + \frac{1}{12}z^2} \quad (72)$$

$$A_{BD_{3,3}} = \frac{1 - \frac{1}{2}z + \frac{1}{10}z^2 - \frac{1}{120}z^3}{1 + \frac{1}{2}z + \frac{1}{12}z^2 + \frac{1}{120}z^3} \quad (73)$$

$$A_{BD_{1,2}} = \frac{1 - \frac{1}{3}z}{1 + \frac{2}{3}z + \frac{1}{6}z^2} \quad (74)$$

$$A_{BD_{2,3}} = \frac{1 - \frac{2}{3}z + \frac{1}{60}z^2}{1 + \frac{3}{5}z + \frac{3}{20}z^2 + \frac{1}{60}z^3} \quad (75)$$

$$A_{BD_{0,2}} = \frac{1}{1 + z + \frac{1}{2}z^2} \quad (76)$$

$$A_{BD_{1,3}} = \frac{1 - \frac{1}{4}z}{1 + \frac{3}{4}z + \frac{1}{4}z^2 + \frac{1}{24}z^3} \quad (77)$$

Comparing the amplification factor $A_{BD_{i,j}}$ to the rational polynomial $R(z)$ of the Padé approximations, namely Eq. 1, implies that the $BD_{j,j}, j = 2, 3$ integrators are spectrally equivalent to the diagonal Padé table entries, the $BD_{j-1,j}, j = 2, 3$ integrators are spectrally equivalent to the first sub-diagonal Padé table entries, and the $BD_{j-2,j}, j = 2, 3$ integrators are spectrally equivalent to the second sub-diagonal Padé table entries. Thus, the $BD_{i,j}$ integrators are unconditionally stable (A -stable). An algorithm is termed to be energy conserving provided that $\lim_{|z| \rightarrow \infty} |A| = 1$. For Eq. 72 and Eq. 73 this can be verified since the highest power of z in the denominator is equal to that highest power of z in the numerator. Thus, we have

$$\begin{aligned} A_{BD_{2,2}}^\infty &= \lim_{|z| \rightarrow \infty} A_{BD_{2,2}} = 1 \\ A_{BD_{3,3}}^\infty &= \lim_{|z| \rightarrow \infty} A_{BD_{3,3}} = -1 \end{aligned} \quad (78)$$

which implies that

$$|A_{BD_{2,2}}^\infty| = |A_{BD_{3,3}}^\infty| = 1 \quad (79)$$

An algorithm is termed to be asymptotically annihilating provided that $\lim_{|z| \rightarrow \infty} |A| = 0$. For Eqs. 74 – 75 and Eqs. 76 – 77 this can be verified since the highest power of z in the denominator is greater than the highest power of z in the numerator. Thus, we have

$$\begin{aligned} \lim_{|z| \rightarrow \infty} |A_{BD_{1,2}}| &= \lim_{|z| \rightarrow \infty} |A_{BD_{0,2}}| = 0 \\ \lim_{|z| \rightarrow \infty} |A_{BD_{2,3}}| &= \lim_{|z| \rightarrow \infty} |A_{BD_{1,3}}| = 0 \end{aligned} \quad (80)$$

This property of the spectral radius monotonically going to zero is also referred to as L -stability [Hairer and Wanner (1991)]. The spectral radius curves for the $BD_{i,j}$ integrators are illustrated in Figs. 6a – 6b. From these figures the energy conserving property of $BD_{j,j}, j = 2, 3$ integrators and asymptotic annihilation property of $BD_{j-1,j}$

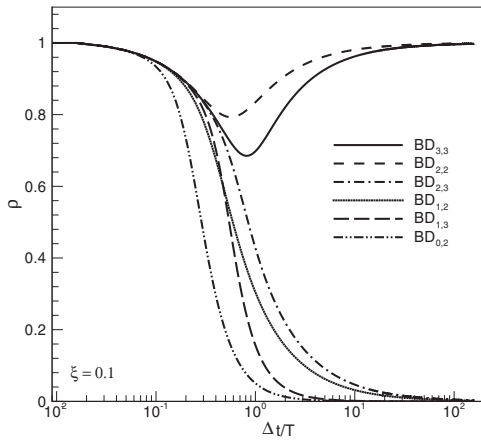
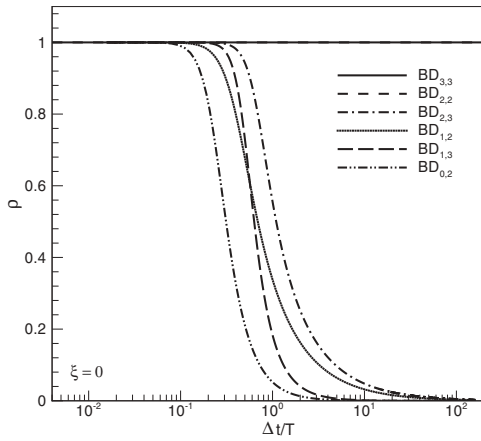


Figure 6 : Spectral radius for bi-discontinuous time integration methods with and without physical damping.

and $BD_{j-2,j}$, $j = 2, 3$ integrators is clearly evident. Figure 6b depicts the spectral radius curve for $BD_{i,j}$ integrators with physical damping ($\xi = 0.1$). From these figures it is clear that the $BD_{j-1,j}$ and $BD_{j-2,j}$ time integration operators remain L -stable and energy dissipating. Whereas the $BD_{j,j}$ time integration operators remain A -stable, however, in the neighborhood of the frequencies associated with $\Delta t/T = 1$ some dissipation is introduced. In the limit as $\Delta t/T \rightarrow \infty$ it is seen that $\rho \rightarrow 1$ for all ξ . A similar behavior is observed for the well known Newmark and the midpoint rule algorithms, which are spectrally equivalent to the Padé rational function $R_{1,1}(z)$.

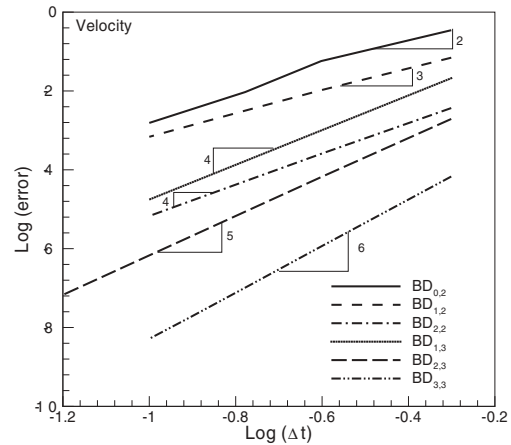
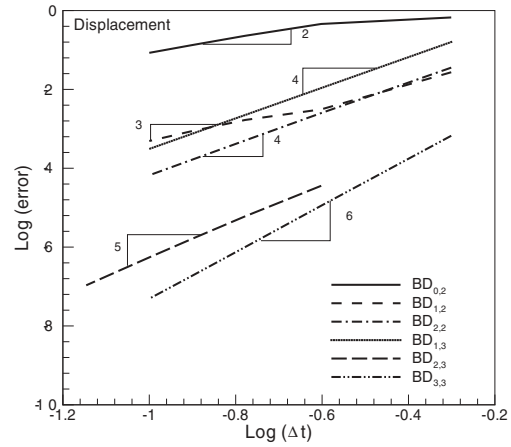


Figure 7 : Convergence analysis of the displacement and the velocity as Δt decreases for bi-discontinuous time integration operators with $f(t) = 0$.

5.2 Consistency

The order of accuracy can be found by determining the leading term of the difference between the exact solution (exponential) and the A_{BD} with respect to the powers of Δt . For the $BD_{i,j}$, $j-2 \leq i \leq j$ time integration operators, we have the following results:

$$BD_{2,2} : (e^{-z} - A_{BD_{2,2}})d_n^- = \frac{-\Delta t^5 z}{720} d_n^- \Rightarrow O(\Delta t^4)$$

$$BD_{3,3} : (e^{-z} - A_{BD_{3,3}})d_n^- = \frac{\Delta t^7 z}{100800} d_n^- \Rightarrow O(\Delta t^6)$$

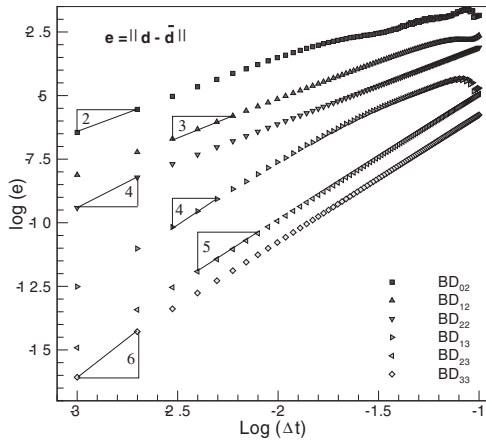


Figure 8 : Convergence analysis of state variable \mathbf{d} , (the displacement and the velocity), as Δt decreases for bi-discontinuous time integration operators with $f(t) = a \cos(\omega t)$.

$$BD_{1,2} : (e^{-z} - A_{BD_{1,2}})d_n^- = \frac{\Delta t^4 z}{72} d_n^- \Rightarrow O(\Delta t^3)$$

$$BD_{2,3} : (e^{-z} - A_{BD_{2,3}})d_n^- = \frac{-\Delta t^6 z}{7200} d_n^- \Rightarrow O(\Delta t^5)$$

$$BD_{0,2} : (e^{-z} - A_{BD_{0,2}})d_n^- = \frac{-\Delta t^3 z}{6} d_n^- \Rightarrow O(\Delta t^2)$$

$$BD_{1,3} : (e^{-z} - A_{BD_{1,3}})d_n^- = \frac{\Delta t^5 z}{480} d_n^- \Rightarrow O(\Delta t^4)$$

Thus, the $BD_{i,j}$ integrators have the order of accuracy equal to $i + j$. That is, they are of the order $2q$, $2q - 1$, and $2q - 2$, respectively, for the $BD_{q,q}$, $BD_{q-1,q}$ and $BD_{q-2,q}$ time integration operators where n is the number of unknowns in the bi-discontinuous weakform, Eq. 23, and hence the number of system solves. To confirm these orders of accuracy of the $BD_{i,j}$ integrators, a undamped single-degree-of-freedom homogeneous system $\ddot{u} + \omega^2 u = 0$ and a non-homogeneous system $\ddot{u} + \omega^2 u = a \cos(\omega t)$ with $u_0 = 1, \dot{u}_0 = 1$ initial conditions and $\omega = \pi$ and $\omega_l = \omega - 1$ is considered. The error at the end of time $t = 0.5$ is computed. Figures. 7 and 8 shows the convergence for the displacement and velocity for the $BD_{i,j}, j = 2, 3; j - 2 \leq i \leq j$ as Δt decreases for homogeneous and non-homogeneous system respectively. As expected, these figures exhibit the theoretical order of convergence. Similarly, the convergence results can be

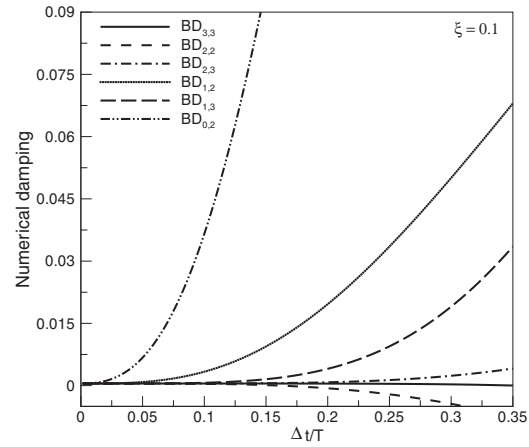
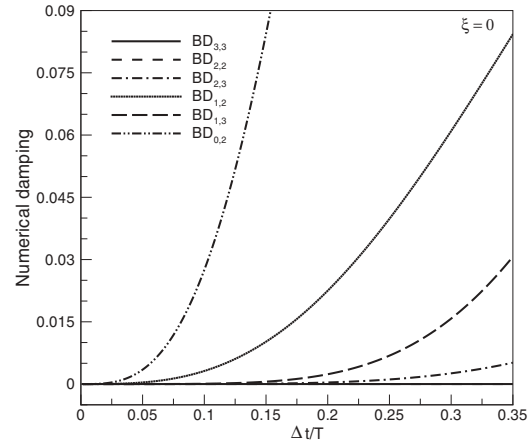


Figure 9 : Numerical dissipation ($\bar{\xi}$ algorithmic damping) for bi-discontinuous (BD) time integration methods with and without physical damping.

readily shown for damped $\xi \neq 0$ system. Note that the time step employed for the study is relatively large compared to the time step considered for the traditional lower order ($\leq O(\Delta t^2)$) time integration operators.

5.3 Numerical Dissipation

Numerical dissipation is also called as algorithmic dissipation or algorithmic damping. This provides a measure of the dissipative effect induced by the algorithm. In order to study the dissipative characteristics of the time integration operators small values of Ω are considered (i.e. for low frequency modes). If the eigenvalues of the \mathbf{A} remain complex conjugate, i.e., we have

$$\lambda_{1,2} = a \pm ib = e^{\overline{\Omega}_D(-\bar{\xi} \pm i)} \quad (81)$$

where $i = \sqrt{-1}$ and $b \neq 0$, then we have

$$\xi_d = \bar{\xi} - \xi = -\frac{\ln(\rho)}{\sqrt{\overline{\Omega}_D^2 + \ln^2(\rho)}} - \xi \approx -\frac{\ln(\rho)}{\overline{\Omega}_D} - \xi \quad (82)$$

$$\overline{\Omega}_D = \arccos\left(\frac{b}{\rho}\right) \quad (83)$$

$$\rho = \sqrt{a^2 + b^2} \quad (84)$$

where ξ is the physical damping, and ξ_d is the algorithmic damping ratio which provides the measure of the numerical dissipation. Figure 9 illustrates the algorithmic damping of the $BD_{i,j}$, $j = 2, 3$, $j-2 \leq i \leq j$ time integration operators.

The function ξ_d is plotted in Fig. 9a for the case without physical damping ($\xi = 0$). The $BD_{j,j}$ time integration operators do not possess any numerical dissipation. The $BD_{j-1,j}$ and the $BD_{j-2,j}$ time integration operators possess numerical dissipation with $BD_{0,2}$ having the highest and $BD_{2,3}$ having the least. It is also evident that with the increase in the order of accuracy of the time integrators, the numerical dissipation decreases. Figure 9b shows the numerical dissipation with physical damping ($\xi = 0.1$). For the $BD_{j,j}$ time integration operators, $\xi_d = \xi$ at $\Delta t/T = 0$ and tends to zero with increasing values of $\Delta t/T$. However, for the $BD_{j-1,j}$ and the $BD_{j-2,j}$ time integration operators, $\xi_d = \xi$ at $\Delta t/T = 0$ and increases with increasing values of $\Delta t/T$.

5.4 Numerical Dispersion

Numerical dispersion is related to the relative period error, which is defined as

$$\frac{\overline{T} - T}{T} = \frac{\Omega}{\overline{\Omega}_D} - 1 \quad (85)$$

where

$$T = \frac{2\pi}{\omega}; \quad \overline{T} = \frac{2\pi}{\overline{\omega}} \quad (86)$$

$$\Omega = \omega\Delta t; \quad \overline{\Omega}_D = \overline{\omega}_D\Delta t \quad (87)$$

The period error without physical damping ($\xi = 0$) is described in Fig. 10a. The $BD_{j,j}$ and $BD_{j-1,j}$ time integration operators have positive period errors. That is, for a

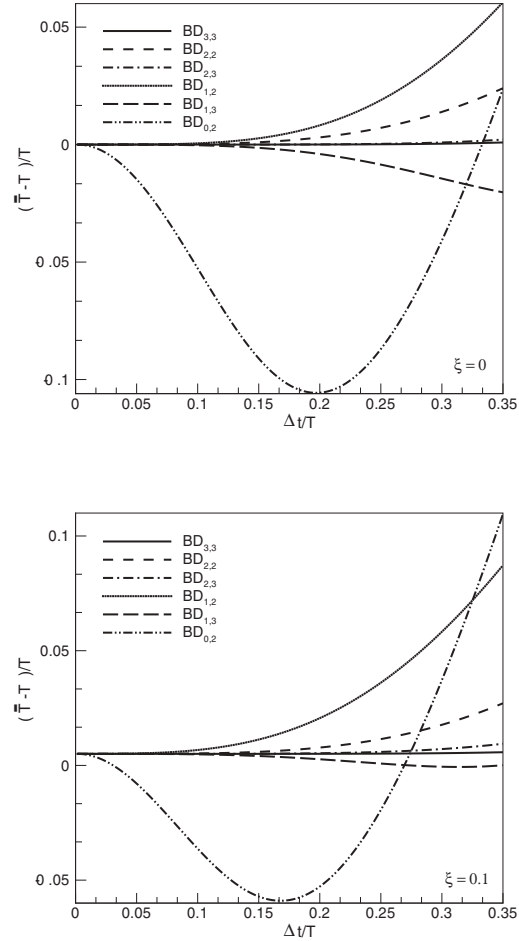


Figure 10 : Numerical dispersion ($(\overline{T} - T)/T$ period error) for bi-discontinuous time integration methods with and without physical damping.

given time step the period of the solution is larger than the actual period. The $BD_{j-2,j}$ time integration operators have a negative period error. In all the cases, the period error is reduced with increase in the order accuracy of of the time integrators. Figure 10b shows the period error with physical damping ($\xi = 0.1$). The above observations still hold with physical damping. However, the errors show a more positive trend in comparison to the error without physical damping for a given $\Delta t/T$.

5.5 Overshoot characteristics

Although an algorithm is unconditionally stable, excessively large oscillations in the displacement and velocity may occur during the first few time steps of the compu-

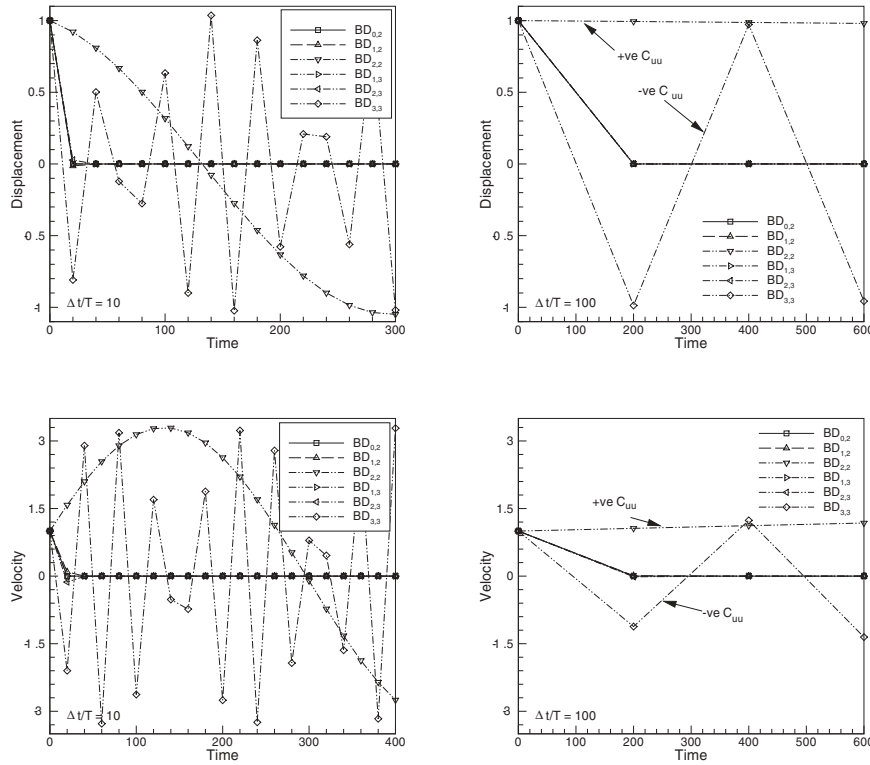


Figure 11 : The displacement and velocity response for large time steps $\Delta t/T = 10$ and $\Delta t/T = 100$ indicates zero-order displacement and zero-order overshoot behavior of bi-discontinuous time integration operators.

tation in the high frequency regime when nonzero initial conditions are imposed. This characteristic which is independent of the stability properties of the time integration operator is termed as the overshoot behavior of the algorithm. To study the overshoot behavior of the time integration operators, undamped, conservative system with non-zero initial conditions in displacement and/or velocity are considered. Then, the solution at the end first time step with $\lim_{\Omega \rightarrow \infty}$ can be represented as

$$u_1 = c_{uu}(\Omega^a)u_0 + c_{uv}(\Omega^b) \dot{u}_0 \tag{88}$$

$$\dot{u}_1 = c_{vu}(\Omega^c)u_0 + c_{vv}(\Omega^d) \dot{u}_0 \tag{89}$$

where the coefficients c_{uu} , c_{uv} , c_{vu} and c_{vv} are functions of $\Omega = \omega\Delta t$. These coefficients contribute to the overshoot behavior of the time integration operators. Thus, to enable zero-order displacement and zero-order velocity overshoot behavior (U0-V0), the powers of Ω , a, b, c, d have to be less than or equal to zero. The coefficients c_{uu} , c_{uv} , c_{vu} and c_{vv} are entries of the amplification matrix at $\lim_{\Omega \rightarrow \infty}$. First, it can be readily proved that the time integration operators $BD_{i,j}$ have zero-order dis-

placement and zero-order velocity overshoot behavior since the Eqs. 78 and 80 are independent of the terms involving z . For structural dynamics, taking

$$z = \begin{bmatrix} 0 & -1 \\ \Omega^2 & 2\xi\Omega \end{bmatrix} \tag{90}$$

and the initial condition vector as

$$d_0 = (u_0, \dot{u}_0 \Delta t)^T \tag{91}$$

and taking the $A_{BD}^\infty = \lim_{\Omega \rightarrow \infty} A_{BD}$, we have the coefficients as listed in the Table 1. From the Table 1 it is clear that all the BD time integration operators have zero-order displacement and zero-order velocity overshoot behavior for no-zero initial conditions as the coefficients are independent of the term $\Omega(z)$. It can also be readily shown that this result is also true for systems with physical damping.

To validate these theoretical results the following experiment is carried out. The responses u and \dot{u} of the single-degree-freedom system, $\ddot{u} + \omega^2 u = 0$ with nonzero initial

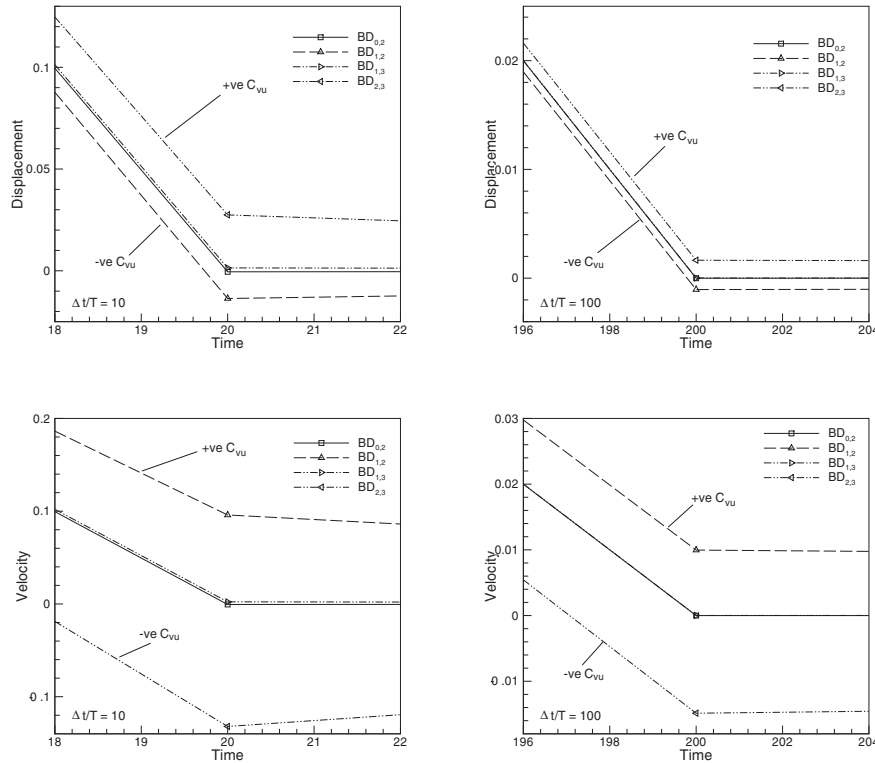


Figure 12 : The displacement and velocity response for large time steps $\Delta t/T = 10$ and $\Delta t/T = 100$ ($T = 2.0$) in the vicinity of end of first time step for BD time integration operators (zoom of Figs. 11a – 11d to illustrate elimination of spurious high-frequency response at the end of first time step).

Table 1 : Overshoot coefficients of the amplification matrix for BD time integration operators.

Time operators	$d_1 = \mathbf{A}_{BD_\infty} d_0$				Remarks
	c_{uu}	c_{uv}	c_{vu}	c_{vv}	
BD _{2,2}	1	0	12	1	Diagonal
BD _{3,3}	-1	0	-24	-1	
BD _{1,2}	0	0	2	0	First sub-diagonal
BD _{2,3}	0	0	-3	0	
BD _{0,2}	0	0	0	0	Second sub-diagonal
BD _{1,3}	0	0	0	0	

conditions $u_0 = 1$ and $\dot{u}_0 = 1$ are recorded for the time step $\Delta t = 10T, 100T$ where T ($T = 2$) is the period of the oscillations. The responses are shown in Fig. 11a – 11b for u and Figs. 11c – 11d for \dot{u} , respectively. Again, it is clear from these figures that the BD time integration operators are zero-order in displacement and zero-order in velocity overshoot behavior. That is, the displacement and velocity responses are bounded with increasing val-

ues of $\Delta t/T \gg 1$.

From the Table 1 and Figs. 11a – 11d and Figs. 12a – 12d the following conclusions can be drawn. All the BD time integration operators are (U0-V0) methods. Only $BD_{j-2,j}$ time integration operators ideally inherit and are asymptotically annihilating operators, i.e., the spurious oscillations in the high-frequency are eliminated at the end of the first time step (see. Figs. 12a – 12d). However, the $BD_{j-1,j}$ time integration operators are only almost to perfect asymptotic annihilating operators, i.e., the spurious oscillations in the high-frequency are eliminated only after the first time step (see Fig. 12a – 12d). While the responses of $BD_{j,j}$ time integration operators are bounded in the high-frequency regime, they possess spurious oscillations which are characterized by the overshoot coefficients c_{uu} , c_{uv} , c_{vu} and c_{vv} . In addition, with the increase in the order of accuracy of the time integrators the value of the overshoot coefficients increases (see. Table 1). This also true for the $BD_{j-1,j}$ time integration operators. However, the effects due to these are negligi-

ble.

6 Conclusions

A mathematical framework and the design leading to a unified set of hierarchical time discontinuous state-phase operators useful for computational dynamics was described. The resulting algorithms fundamentally inherit good algorithmic attributes, and the framework provides for the first time the simultaneous design of a unified set of energy conserving/dissipating time integration operators. Lastly, all the time operators in the present context naturally inherit a hierarchical structure that is useful for time adaptive computations.

Acknowledgement: The authors are very pleased to acknowledge support in part by Battelle/U. S. Army Research Office (ARO) Research Triangle Park, North Carolina, under grant number DAAH04-96-C-0086, and by the Army High Performance Computing Research Center (AHPCRC) under the auspices of the Department of the Army, Army Research Laboratory (ARL) under contact number DAAD19-01-2-0014. The content does not necessarily reflect the position or the policy of the government, and no official endorsement should be inferred. Support in part by Dr. Andrew Mark and Dr. Raju Namburu is also gratefully acknowledged. Special thanks are due to the CIS Directorate at the U. S. Army Research Laboratory (ARL), Aberdeen Proving Ground, Maryland. Other related support in form of computer grants from the Minnesota Supercomputer Institute (MSI), Minneapolis, Minnesota is also gratefully acknowledged.

References

- Borri, M.; Bottasso, C.** (1993): A General Framework for Interpreting Time Finite Element Formulations. *Computational Mechanics*, vol. 13, pp. 133–142.
- Borri, M.; Mello, F. J.; Atluri, S. N.** (1978): Variational Approaches for Dynamics and Time-Finite-Elements: Numerical Studies. *Comp. Mech.*, vol. 7, pp. 49–76.
- Chien, C.-C.; Wu, T.-Y.** (2001): An Advanced Time-Discontinuous Galerkin Finite Element Method for Structural Dynamics. *CMES: Computer Modeling in Engineering and Sciences*, vol. 2, no. 2, pp. 213–226.
- Ehle, B. L.** (1969): On Padé Approximations to the Exponential Function and A-stable Methods for the Numerical Solution of Initial Value Problems. Technical Report CSRR 2010, University of Waterloo, Dept. AACS, 1969.
- Fung, T. C.; Leung, A. Y. T.** (1996): On the Accuracy of Discontinuous Galerkin Methods in the Time Domain. *Journal of Vibration and Control*, vol. 2, pp. 193–217.
- Gragg, W. B.** (1972): The Padé table and its relation to certain algorithms of numerical analysis. *SIAM Rev.*, pp. 1–62.
- Hairer, E.; Wanner, G.** (1991): *Solving Ordinary Differential Equations II: Stiff and Differential-Algebraic Problems*. Springer-Verlag, New York.
- Hairer, E.; Wanner, G.** (2000): Order Stars and Stiff Integrators. *Journal of Computational and Applied Mathematics*, vol. 125, pp. 93–105.
- Hulbert, G. M.** (1992): Time Finite Element Methods for Structural Dynamics. *Int. J. Numer. Methods Engrg.*, vol. 33, pp. 307–331.
- Li, X. D.; Wiberg, N.-E.** (1996): Structural Dynamic Analysis by a Time-Discontinuous Galerkin Finite Element Method. *Int. J. Numer. Methods Engrg.*, vol. 39, pp. 2131–2152.
- Mello, F. J.; Borri, M.; Atluri, S. N.** (1990): Time Finite Element Methods for Large Rotational Dynamics of Multi-body Systems. *Computers and Structures*, vol. 37, pp. 231–240.
- Moller, P. W.** (1993): High-Order Hierarchical A- and L-Stable Integration Methods. *Int. J. Numer. Methods Engrg.*, vol. 36, pp. 2607–2624.
- Tamma, K. K.; Zhou, X.; Sha, D.** (2000): The Time Dimension: A Theory of Development/Evolution, Classification, Characterization, and Design of Computational Algorithms for Transient/Dynamic Applications. *Archives of Computational Methods in Engineering*, vol. 7, pp. 67–290.
- Wiberg, N.-E.; Li, X. D.** (1996): Adaptive Finite Element Procedures for Linear and Non-linear Dynamics. *Int. J. Numer. Methods Engrg.*, vol. 46, pp. 1781–1802.